JOURNAL OF COMPUTATIONAL PHYSICS 51, 484–501 (1983)

Implicit Moment PIC-Hybrid Simulation of Collisional Plasmas*

RODNEY J. MASON

Los Alamos National Laboratory, Los Alamos, New Mexico 87545

Received June 15, 1982; revised January 4, 1983

A self-consistent scheme was developed to model electron transport in evolving plasmas of arbitrary classical collisionality. The electrons and ions are treated as either multiple Eulerian fluids or collisional particles-in-cell. Particle suprathermal electrons scatter off ions, and drag against fluid background thermal electrons. The background electrons undergo ion friction, thermal coupling, and bremsstrahlung. The components accelerate in electric fields obtained by the Implicit Moment Method, which permits $\Delta t \gg \omega_p^{-1}$ and $\Delta x \gg \lambda_D$—allowing the treatment of problems 10^2–10^3 times more complex than those accessible with older explicit methods. The fluid description for the background plasma components permits the modeling of transport in systems spanning more than a 10^7-fold change in density, and encompassing contiguous collisional and collisionless regions. Results are presented from application of the scheme to the modeling of CO_2 laser-generated suprathermal electron transport in expanding thin foils, and in multi-foil target configurations.

1. INTRODUCTION

At laser wavelengths exceeding 0.5 μm a significant fraction of the light absorbed by laser fusion targets is deposited in suprathermal electrons. These are marginally collisional and distribute the absorbed energy throughout the target. As they move, they set up self-consistent electric fields which draw return currents in the background, generally strongly collisional, thermal electrons. These fields also set the ions into motion, changing the target geometry, in which the suprathermals must transport. A detailed model of this complex coupled phenomenology is required if we are to develop the intuition and understanding needed to engineer the use of suprathermals in the design of targets for high compression. Here, our efforts toward the development of such a model were confined to a one-dimensional treatment. However, our choice of approach has been guided by the ease with which it might be generalized to higher dimensions.

*This work was performed under the auspices of the United States Department of Energy. The U.S. Government's right to retain a nonexclusive royalty-free license in and to the copyright covering this paper, for governmental purposes, is acknowledged.

0021-9991/83 $3.00

Thus, we treat the suprathermal electrons as collisional particles-in-cell. The particle-in-cell (PIC) approach [1] has established reliability in application to collisionless modeling in one and two dimensions. Motion in self-consistent fields presents no difficulty. The weak effects of ion scatter and electron drag are readily added with the inclusion of simple operators on the suprathermal velocities. The collisional PIC treatment for the suprathermals has been previously outlined in [2] and [3]. Shanny *et al.* [4] were the first to use the electron-ion scattering procedure.

The return current thermal electrons are moved as a collisional Eulerian fluid. This allows us to treat the very large range of densities characterizing the solid, the critical region and the tenuous target corona. The resistive force between the thermal electrons and ions is handled implicitly, so strong collisionality simply leads to low relative drift speeds. The fluctuations of a particle background representation are avoided. Similarly, the ions are modeled as a fluid. To advance the fluids we use the donor-cell prescription given by Gentry *et al.* [5], with flux-correction improvements to reduce numerical diffusion, as recommended by Book *et al.* [6] and Zalesak [7].

The electrons and ions move in self-consistent electric fields calculated by the Implicit Moment Technique. For this an auxiliary set of fluid equations is solved implicitly with the Poisson equation to give an advanced field. By moving the electron and ion components in this field, we avoid the usual time-step constraint to steps less than the minimum plasma period. Thus, global problems spanning a large density range can be run as much as a thousand times faster than by traditional explicit methods. A rudimentary form of the Implicit Moment Technique for the electric field is found in [2]. We provide a more rigorous and complete discussion in [8]. Related implicit field methods have been explored by Denavit [9] and by Friedman *et al.* [10].

Although a multi-group treatment of the suprathermals would be computationally more efficient, we avoid it to skirt the need for suprathermal flux-limitation in collisionless regions, and anticipating later difficulties in extending a self-consistent multi-group treatment to higher dimensions. Forslund and Brackbill [11] have shown that Implicit Moment Particle Simulation readily extends to two dimensions. An Eulerian description was chosen for the fluids to provide compatibility with the field and particle descriptions on a fixed orthogonal mesh.

In Section 2 we will detail the important features of our computational model. The collisional PIC suprathermal approach will be reiterated. The modifications in the standard donor-cell procedures needed to allow for two-fluid collisional hydrodynamics (colliding thermal electrons and ions) will be stressed, as will the techniques needed to reduce numerical diffusion. Also, we will focus on the changes in the Implicit Moment Technique demanded by the presence of collisions and the simultaneous use of both particle and fluid hydrodynamic descriptions for the plasma components. Then, in Section 3 we provide sample applications of the net transport scheme to the motion of suprathermals through thin and thick single foils, as well as double-foil target configurations, as might be used for vacuum insulation. The concluding Section 4 summarizes our findings, and recommends future directions.

2. The Computational Model

A. *Suprathermal Electron Particles*

(*a*) *Emission and motion.* The modeling begins with an initially prescribed background plasma of thermal electrons and ions. These are described on a one-dimensional mesh of typically 100 cells. At some prescribed location, suprathermal (or hot) electrons are emitted. This location is preset for certain test problems or chosen by operations which follow laser light up to the critical surface, which then becomes a moving emission point for the suprathermals. As these hot electrons are produced, the background density of thermal (or cold) electrons is correspondingly reduced. The suprathermals are given a longitudinal velocity u, and carry a transverse speed v. When the hot emission is meant to mock-up resonance absorption, the electrons are given an average drifting Maxwellian distribution in a 20° cone about the direction toward the laser. Their x-directed temperature (mean energy) is given by the Forslund formula [12], $T_{hx} \sim (I\lambda)^{1/3}\, T_c^{1/3}$, in accordance with experiment and theory. The transverse temperature characterizing the average v is then taken as $T_{hx} \sin^2(20°/180°\pi)$. For certain tests the dependence on the cold background temperature T_c may be neglected, or T_{hx} may simply be fixed. The emitted density of each cycle is adjusted so that the new suprathermals carry off the requisite absorbed energy.

Typically, two electrons are emitted each computational cycle. Their velocities are changed by drag and scattering operators, and then they are moved according to

$$u^{(m+1)} = u^{(m)} + \frac{q_\alpha E^{(*)}}{m} \Delta t, \tag{1a}$$

$$x^{(m+1)} = x^{(m)} + u^{(*)}\, \Delta t. \tag{1b}$$

Here $u^{(*)}$ and $E^{(*)}$ are appropriately centered choices for the drift velocity and field. At present to ensure the greatest numerical stability and simplify the model, for $(*)$ we use level $(m+1)$.

(*b*) *Drag.* Coulomb drag slows the suprathermals against the background electrons. To model this we reduce the hot speeds during each cycle by

$$\Delta c = \frac{-4\pi e^4 n_i}{mkT_e} \Delta t\, G(\xi) \log \lambda, \qquad \xi = \left(\frac{mc^2}{2kT_e}\right)^{1/2}, \tag{2a}$$

in which

$$G(\xi) = \frac{0.376\xi}{(1 + 0.542\xi - 0.504\xi^2 + 0.752\xi^3)} \tag{2b}$$

is a polynomial fit [13] to Spitzer's error function combination, and $c^2 = u^2 + v^2$; again, v is perpendicular to u. Thus, the drag goes as c^{-2} for large speeds, as in [2].

It peaks at $\xi = 1$ and is zero as $c \to 0$. Energy dragged from the suprathermals is redeposited locally in the thermals, raising T_c. At present the lost momentum is discarded. To avoid non-physical thermal heating as the hot electrons reflect in the corona, the drag is suppressed for $n_h > n_c$. Otherwise, when the energy of a hot electron is dragged below kT_c, the slow hot electron is destroyed, with its density and energy attributed to the thermal electron background. In sufficiently collisional problems a semi-equilibrium situation can be established, in which the hot electrons created by the resonant absorption process are eventually all destroyed by the drag, and the number of simulation particles needed to describe the suprathermals in flight is relatively constant.

(*c*) *Scatter.* It is assumed that each hot electron undergoes many small angle deflections on crossing a finite thickness of plasma. Since the successive collisions are independent events, the central limit theorem indicates that for Rutherford scattering, the distribution $P(\theta)$ of net deflection angles, $\theta \geqslant 0$ from the original forward direction for each electron, will be approximately Gaussian [2, 4], i.e.,

$$P(\theta) = \frac{\theta}{\langle \theta^2 \rangle} \exp\left(\frac{-\theta^2}{2\langle \theta^2 \rangle}\right) \tag{3}$$

with $\langle \theta^2 \rangle = 8\pi e^4 m^{-2} c^{-3} \Delta t n_i Z(Z+1) \log \lambda$. In the $Z+1$ factor the Z accounts for scatter off ions and the $+1$ term approximates the effect of scatter off electrons. In each time step, random numbers are picked from a list of 10^4 pre-established random numbers and used to pick a new θ and a new uniformly distributed azimuthal angle ψ. The use of this random list speeds the angular selection process by a factor of about 3, at the cost of minor error in the randomness. Overall, in an angular scattering event the velocity vector of a suprathermal is simply rotated, while its energy is conserved. The trigonometry associated with these rotations is detailed in [2]. When the background density is sufficiently low, or when an electron is sufficiently energetic, $\langle \theta^2 \rangle \ll 1$, and the electron is essentially undeflected during a time step. Then there is also minimal drag, so that the motion of the electron is essentially that of conventional, fully-deterministic PIC.

On the average, this scattering procedure gives an effective collision frequency for the suprathermals of $\nu_h = \langle \theta^2 \rangle / (2\Delta t)$, where ν_h is the rate of mean momentum loss from friction against the ions and background electrons. As formulated, our scattering procedure is valid only so long as $\nu_h \Delta t \leqslant 1$. For longer time steps the particle motion should become a random walk, with the total distance traversed during a time step significantly reduced below $u\Delta t$. The problem of finding a particle collision treatment, uniformly valid for arbitrary $\nu_h \Delta t$, is akin to the need in two-dimensional modeling [11] for a uniform implicit particle technique for arbitrary ω_c values (where ω_c is the electron cyclotron frequency). Both developments warrant further work. Some progress has been made in restricting the particle excursions in the presence of very frequent collisions to the limits imposed by Brownian motion [3], but for the present model we choose, instead, to treat the more collisional

electrons as a thermal fluid. Conversion of the strongly collisional hot electrons to thermals in the drag modeling generally obviates the need for scrutiny of the $\nu_h \Delta t < 1$ requirement in the application of the model to CO_2-generated suprathermal transport.

B. Thermal Electron and Ion Fluids

A fluid treatment is needed for the background plasma in order to model strongly collisional regions, but also to manage the very large range of densities encountered in laser-target simulations. When 100 particles per cell are used to represent the peak density region of a foil, the lowest density resolvable is 1/100th of the peak. Fully ionized gold at solid density represents about 4×10^{24} electrons/cm^3, so with this small simulation particle density only regions down to 4×10^{22} could be explored, while the critical density for CO_2 is 10^{19}/cm^3, and modeling of transport in the contiguous solid and critical regions could prove crucial to important pellet designs. This limit to resolution presents no difficulty in the hot electron modeling, since the laser tends to establish a peak hot electron density on the order of 10^{19}/cm^3, and there is little need to model them in regions where their density drops below 10^{17}.

We use an extension of Braginskii's equations [14] for the two-fluid background plasma. For fixed ions this extension is given in [2]. We solve the fluid equations using a variation on the donor-cell procedure of Gentry *et al.* [5]. At each time step the hydrodynamics is divided into a "Lagrangian" and then an "advection" phase. During the Lagrangian phase the fluid velocities are advanced by the local pressure gradients and electric fields. The resistive terms in the momentum equations are treated implicitly, so that strong collisions directly imply diffusion of the cold thermals through the ions. Similarly, during this phase the fluids do hydrodynamic work, and the electrons are Joule heated, while receiving energy from the dragged suprathermals. We store the cold electron and ion densities and temperatures $n_{c,i}$ and $T_{c,i}$ at the cell centers. The velocities $u_{c,i}$ are stored at the boundaries. During the advection phase this information is moved to the neighboring centers and boundaries.

When the ions can move, the thermal electrons should drift at the local ion speed in strongly collisional regions. Thus, for the differenced coupled momentum equations, we use

$$j_{h,c}^{(m+1)} = j_{h,c}^{(m)} - \frac{1}{m}\frac{\partial \Pi_{h,c}^{(m)}}{\partial x}\Delta t - \frac{e n_{h,c} E^{(*)} \Delta t}{m} - \nu_{h,c}\Delta t \left(j_{h,c}^{(m+1)} - \frac{n_{h,c} j_i^{(m)}}{n_i} \right), \tag{4a, b}$$

$$j_i^{(m+1)} = j_i^{(m)} - \frac{1}{M}\frac{\partial \Pi_i^{(m)}}{\partial x}\Delta t + \frac{Z e n_i E^{(*)} \Delta t}{M} - \left(\nu_h \Delta t \frac{n_h}{n_i} + \nu_c \Delta t \frac{n_c}{n_i} \right) \frac{m}{M} j_i^{(m)} + \nu_h \Delta t \frac{m}{M} j_h^{(m+1)} + \nu_c \Delta t \frac{m}{M} j_c^{(m+1)} \tag{4c}$$

when thermoelectric effects [2] are neglected. Here Π is the total pressure, e.g., for

the electrons $\Pi = n(mU^2 + kT) + P_a$, and, of course, $j \equiv nU$; P_a is a Von-Neuman artificial viscosity. Again, (*) implies $(m + 1)$. The j_h equation is, for the most part, redundant, being used here to render explicit the information needed in the collision term for the ion momentum equation. The level (m) hot electron moment data is obtained from PIC accumulations [1]. The collision rates $\nu = 1/\tau$ are from Braginskii, as in [2] with $T \to (T + mU^2/3k)$, including the U^2 to approximate the effect of large drift velocities. The j_i elements in the collision terms are left at level (m) to simplify the algebra in the solutions for $j_{c,i}^{(m+1)}$. This restricts the model to moderately collisional regimes, such that the product $\nu \Delta t\ m/M \ll 1$. We store the ν values at cell centers, and E at cell boundaries. For Eqs. (4) we construct Π for the centers, and boundary-average the n and ν values.

For the Lagrangian phase of the hydrodynamic calculation we solve Eqs. (4) for $j_{c,i}$, attributed to cell boundaries. Intermediate boundary velocities are then obtained from $U(i + 1/2)^{(m+1)} \equiv j^{(m+1)}/n(i + 1/2)^{(m)}$, with $n(i + 1/2) \equiv 0.5(n(i) + n(i + 1))$. The mU^2 terms are suppressed in Π during this phase, but the artificial viscous pressure is retained. In the $\nu_c \Delta t \gg 1$ limit the solution to Eqs. (4) for j_c becomes

$$j_c(m + 1) = -\frac{1}{m\nu_c} \frac{\partial \Pi_c^{(m)}}{\partial x} + n_c U_i^{(m)} - \frac{e n_c E^{(*)}}{m\nu_c}, \tag{5}$$

which is equivalent to an Ohm's law. This will let U_c differ from U_i, as a result of particle diffusion or an external electric field.

The advection is then carried out by moving n and nT across the boundaries from the donating cells, as determined by the sign of $U(i + 1/2)$. Thermal energy nT is advected, rather than total energy, to improve the accuracy of the T determinations (upon which resistivity strongly depends) at the expense of accuracy in the energy conservation. Boundary momentum $n(i + 1/2)\, U(i + 1/2)$ is moved using the average velocity at cell centers. The advection is then completed with an anti-diffusive flux corrective calculation [6, 7] to sharpen the fluid profiles. This substitutes a second-order interpolated donor-cell [15] solution for the first-order (in space) donor-cell solution, wherever this can be done without producing non-physical maxima in the results.

We found that the Eulerian fluid calculations did a poor job of modeling the adiabatic expansion of foils, even with the addition of the FCT anti-diffusive corrections, until special care was taken at vacuum boundaries. First order Eulerian calculations tend to diffuse vacuum interface information across a mesh at a rate of one cell per cycle. This can manifest itself as a persistence of high material temperatures at the edges of an expanding adiabatic flow (essentially the initial temperatures) where $T \sim n^{2/3}$ should be expected. There can also be extreme temperature spikes at the edges, as the calculations effectively register shock heating of the vacuum. An extrapolation of the cell-centered velocities out into the vacuum [16] was found to eliminate most of such spikes (by supressing any compressive heating there). Then, the implementation of FCT [6, 7] was found to stop most of the numerical diffusion of temperature. Remaining small edge spikes in n and T were

removed by a "gating" operation, by which the edge velocity was set to zero until the density behind it reached a value extrapolated from the interior of the material. Note that for two-temperature expansions, in which hot electrons drive the expansion of a low density fast ion edge, the "gate" for the ions must open when the ion density first exceeds an extrapolation of the hot electron density.

The thermal electron temperature T_c is increased as a result of deposition by suprathermals, and propagated via classically limited conduction. In dense collisional regions the thermal electron and ion temperatures will equilibrate; there will also be some radiative emission. We model this, following the hydrodynamic advancement of the fluids, by implicitly coupling T_c to T_i at the Spitzer [17] rate, and similarly by decreasing T_c by bremsstrahlung loss, limited locally to the blackbody emission rate.

C. The Implicit Moment Electric Field

Traditionally, a solution for the electric field through the Poisson equation would restrict calculations to time steps less than the minimum local plasma period on the simulational mesh. We surmount this problem by the Implicit Moment Method [2, 8], by which we introduce auxiliary fluid equations which are solved in conjunction with the Poisson equation for the advanced field $E^{(m+1)}$. Explicit particle and fluid advances are stable in the advanced field for time steps constrained only by a Courant condition on the hottest electrons [8, 9, 11]. For global problems this procedure permits time steps typically 10^3 times larger than those required by earlier methods.

Thus, integrating the Poisson equation in space for time level $(m+1)$,

$$E^{(m+1)} = 4\pi \int_0^x \sum_\alpha q_\alpha \tilde{n}_\alpha^{(m+1)}\, dx + E^{(m+1)}(0), \tag{6}$$

and obtaining densities $\tilde{n}_\alpha^{(m+1)}$ by integrating the continuity equation in time for each species, i.e.,

$$\tilde{n}_\alpha^{(m+1)} = n_\alpha^{(m)} - \frac{\partial}{\partial x}(j_\alpha^{(*)})\,\Delta t, \tag{7}$$

we employ the currents $j_a^{(*)} \equiv j_a^{(m+1)}$ in Eq. (7) from the solutions to Eqs. (4), and obtain

$$E^{(m+1)} = \frac{4\pi\{\int_0^x \sum q_\alpha n_\alpha^{(m)}\, dx - \sum q_\alpha g_\alpha \Delta t\}}{(1+\omega_{pe}^2(\Delta t)^2)} \tag{8a}$$

for the electric field, when $E(0) = j_\alpha = 0$—as for a quiescent left boundary. Here

$$\omega_{pe}^2 = \frac{4\pi e^2}{m}\left(n_h c_h + n_c c_c + Z^2 \frac{m}{M} n_i c_i\right), \tag{8b}$$

$$g_{h,c} = c_{h,c}\left\{j_{h,c}^{(m)} - \frac{1}{m}\frac{\partial \Pi_{h,c}^{(m)}}{\partial x}\Delta t + a_{h,c}\frac{n_{h,c}}{n_i} j_i^{(m)}\right\}, \tag{8c}$$

$$g_i = j_i^{(m)} \left[1 - \left\{ a_h \frac{n_h}{n_i} + a_c \frac{n_c}{n_i} \right\} \frac{m}{M} \right] + \{ a_h g_h + a_c g_c \} \frac{m}{M} - \frac{1}{M} \frac{\partial \Pi_i^{(m)}}{\partial x} \Delta t, \tag{8d}$$

and $a_{h,c} = v_{h,c} \Delta t$, so

$$c_{h,c} = \frac{1}{1 + a_{h,c}}, \qquad c_i = 1 - \left(a_h c_h \frac{n_h}{n_i} + a_c c_c \frac{n_c}{n_i} \right) \frac{1}{Z}. \tag{8e}$$

Moreover, (q_α, m_α) is $(-e, m)$ for the electrons and (Ze, M) for the ions.

In the collisionless limit Eq. (8a) becomes

$$E^{(m+1)} = \frac{4\pi \{ \int_0^x \sum q_\alpha n_\alpha^{(m)} \, dx - \sum q_\alpha j_\alpha^{(m)} \Delta t + \sum q_\alpha / m_\alpha \, \partial \prod_\alpha^{(m)} / \partial x \, (\Delta t)^2 \}}{(1 + \omega_{p0}^2 (\Delta t)^2)}, \tag{9}$$

in which

$$\omega_{p0}^2 = \frac{4\pi e^2}{m} \left[n_e + \frac{m}{M} Z^2 n_i \right].$$

In the quasi-neutral limit, where $\omega_{p0}^2 \Delta t^2 \gg 1$, and when $m/M \ll 1$, Eq. (9) reduces to $E \simeq -1/e n_e \, \partial P_e / \partial x$, where $n_e = n_h + n_c$ and $P_e = P_h + P_c$, plus the summational density and current "correction" terms [8], which help to maintain the charge neutrality. Alternatively, when $\omega_{p0}^2 \Delta t^2 \ll 1$ the field reduces to the Poisson result, i.e., the integral over the sum of the old charge densities $q_\alpha n_\alpha^{(m)}$.

In dense collisional regions Eqs. (8) essentially reduce to Eq. (5), the Ohm's law. Furthermore, when $U_i = 0$, by quasi-neutrality $j_c \simeq j_h$, so that in dense interior regions of a target where the hot electrons are essentially undeflected by collisions or the fields, $j_h^{(m+1)} \simeq j_h^{(m)}$, and thus through Eq. (5) the electric field is determined essentially from the old hot current.

The full electric field equations, Eqs. (8), are basically Eqs. (22) of the Moment Method of [2], except that charge separation effects are now retained through the use of the continuity equation, Eq. (7). The collisionless result has been given in [8] and explored by Denavit in [9]. Its extension to two-dimensions is accomplished in [11].

In the auxiliary fluid equations for the electric field solution, Eqs. (7) and (8), we retain the dynamic pressure contributions $m_\alpha n_\alpha U_\alpha^2$ at the old time level (m). This allows us to accomplish the field solution by a simple algebraic rearrangement of the equations. On the other hand, this same term must be extracted and treated in the separate advective stage of the thermal electron and ion advancement schemes in order to assure hydrodynamic stability. Moreover, at the vacuum edge of the fluid the advection must be done by the donor-cell technique, i.e., material must be drawn from the donating cell established by the cell's boundary velocity so as to assure positivity of the fluid number densities. When the hot electrons enter a boundary

region, for example, the resultant electric field will draw the cold electrons out, and their density must go no lower than zero. This positivity is guaranteed by the donor-cell hydrodynamics. However, a corresponding careful use of donor cells in the auxiliary hydrodynamic equations for the electric field solution would mean that the mnU^2 terms would not be known until E itself was known, and this would clearly require iteration to solve for E. This iteration can be performed, as in the pure particle case [11], but, as yet, we have found no instance when it was needed. We simply use the old dynamic pressures, and restrict our time steps by a Courant limit on the hottest component. The resultant slight difference between the hydrodynamic equations used for the electric field determination and the hydrodynamic procedures then used for the actual fluid advancement appears to cause no non-physical consequences. A very similar incompatibility exists in the fluid equations used to represent the hot electrons in the electric field solution and the set of particle equations actually used to advance the hot electron properties. The fluid equations can be arranged to closely mimic the motions of the particles on the average [11], but the agreement is never perfect, nor has this proven to be necessary. We note that the time required for the algebraic solution for E is negligible, compared to the time needed to advance the fluids and particles.

D. The Multi-Fluid Hybrid Approach

The net system derived for transport studies has great versatility. For tests the hot emission can be suppressed, the electron-ion thermal coupling can be skipped, the thermal conduction can be neglected, and the thermal scattering rate ν_c and the electric field E can be artificially set to zero. Then in foil geometries, for example, the thermal electron and ion fluids expand entirely separately. If the ion mass is made artificially equal to the electron mass with $T_c = T_i$ the two fluids expand in superposition—all their properties are identical. Alternatively, at the physical mass ratio the electron expansion is well ahead of the ion expansion, until the scattering or field are restored. When just the scattering is "on," the electrons are locked into motion with the ions, except at the leading edge of the expansion, where electrons can diffuse ahead. With the field "on," the electrons and ions expand together at the ion acoustic rate [18]. Restoration of the electron-ion thermal coupling gives the ions and cold

[redacted]

of the thermals is evident. The aim of the modeling is to study this highly coupled phenomenology in evolving one-dimensional geometries.

E. Numerical Considerations

(*a*) *The Courant-limited time step.* The reader should note that, while a large time step $\omega_p \Delta t \gg 1$ is permitted with this model, it remains constrained by a Courant condition on the fastest electrons, i.e., $\Delta t < \Delta x/a$ with $a \equiv \sqrt{(kT_{hx}/m)}$, so that with $k \sim 1/\Delta x$, $ka\Delta t < 1$. Since the Debye length λ_D is a/ω_p, this implies that $\Delta x \gg \lambda_D$ also limits the simulations. The Courant limit is required for stability, although this can be

provided at larger time steps if the pressure is made implicit [8, 11]. More particularly, it is needed for accuracy—in describing particle trapping [9], for example. Still, sufficient accuracy may prove possible at larger Δt by the use of subcycling [2, 19].

Relatedly, we observe that Brackbill and Forslund [11] have found that Δt must exceed $0.1\,\Delta x/a$ in full-particle implicit calculations in order to minimize particle heating by the finite grid instability. This can establish a lower bound on the background temperatures accessible to simulation. Our hybrid scheme avoids this lower bound, since a fluid for the background can manifest no finite grid heating.

Our electron Courant time step is at least 43, i.e., $\sqrt{(m/M)}$, times smaller than the normal Courant time step for the ions. Collisions force no further reduction of the time step, since both the thermal electron-ion momentum and energy exchange are treated implicitly. Thus, while our hybrid scheme can be much faster than traditional explicit PIC techniques, its use is still costly. It should be valuable where multi-group descriptions are suspect, e.g., in weakly collisional regions, where diffusion requires flux-limitation (these are particularly prevalent in CO_2-illuminated targets), and where collisionless regions are contiguous with dense collisional ones—with the interaction of these regions of interest. Further, in its extension to two dimensions, the hybrid scheme may prove faster than multi-group diffusion by avoiding the need for costly multiple matrix inversions.

(*b*) *The fluid background.* Generally, the background plasma is dense and cold enough, so that the thermal electrons are strongly collisionally coupled to the ions. The dominant ion motion consists of slow expansions and shocks. Our first order in Δt fluid description is sufficient for the modeling of such mild motions, with the artificial viscosity and *limited* flux-correction [7] providing the necessary shock dissipation. Even if the thermal scattering rate of ions is low (either artificially, or due to a high T_e), the dominant electron motion is a low-speed drift toward the laser spot—so as to supply source electrons for the hot emission. Thus, again the present hydrodynamic scheme should be sufficient.

However, in regions where the cold density has dropped enough to approach the hot electron density, the two components may couple through plasma oscillations and instabilities. For such regions one could improve the model by destroying the local thermal electron fluid and replacing it with additional suprathermals, emitted in a local Maxwellian distribution [3]. Alternatively, one might introduce procedures minimizing in such regions the artificial viscosity and FCT limiting—as numerical stability allows. With removal of the limiting, the resultant scheme becomes pure, second order in space, interpolated donor-cell hydrodynamics [7, 15].

Further, one might choose to extend the fluid descriptions so that the effective γ law for adiabatic expansions, $P \sim n^{\gamma}$, switches with minimal collisions between $\gamma = 5/3$ and $\gamma = 3$. This might be accomplished by retaining separate axial and transverse temperatures in the improved model, and equilibrating these at the local collisional rate—taking target geometry and magnetic fields into consideration in any two-dimensional extension.

(c) *Time centering.* With the present first-order Δt centering, the net transport scheme is stable, simple and robust. The motion of superthermals is largely ballistic and, therefore, energy conservative. However, the suprathermals will reflect periodically off confining fields at vacuum interfaces. Phase space plots show that some 5 to 7% of the particle energy is lost per early bounce—until the electric fields rise to their evolving quasi-neutral values. Energy conservation with such reflections can be improved by using the nearly centered currents, $j_\alpha^{(*)} = \Theta j_\alpha^{(m+1)} + (1-\Theta) j_\alpha^{(m)}$, $\theta = 0.55$ in the continuity equation (7), and, correspondingly, $u^{(*)} = \Theta u^{(m+1)} + (1-\Theta) u^{(m)}$ in Eq. (1b). For $\omega_p \Delta t \gg 1$, this will force $j_\alpha^{(m+1/2)} \to 0$, so $j_\alpha^{(m+1)} \to -j_\alpha^{(m)}$, reversing any drift velocity at vacuum edges—rather than supressing it, as when (*) implies $(m+1)$. Further improvement should come from using $E^{(*)} = E^{(m+\theta)}$ in Eqs. (1b) and (4), and by breaking the hydrodynamics into two steps, with the first establishing half-time fluxes. The higher-order schemes of [9] and [10] are also available, but are avoided here because of the additional complexity present with the fluid background descriptions.

3. Sample Applications

In the sample runs which follow we explore the axial transport in single and multiple foils. In all cases the calculations used 100 cells with equal $\Delta x = 2.4\,\mu$m for a total test area of $240\,\mu$m. The hot electron temperature ranged from 25 to 150 keV. With the 150-keV suprathermals, the time step used was $\Delta t = 0.002$ ps, and the longest runs continued for 2900 cycles to 5.8 ps. These runs took approximately 5 min of CRAY I time. This time step was about four times smaller than that required by electrons moving at twice the hot thermal velocity, so runs to 24 ps could have been made at reduced accuracy in the same CRAY time. Furthermore, no effort has been made to either machine-code or vectorize the operations, so a further three- to fivefold decrease in running time should be readily possible. Two particles were emitted each cycle; consequently, in the absence of drag absorption, 5800 particles were circulating at the end of each long run.

In the simulations we look at the evolution of electron densities ranging from 4×10^{24} cm^{-3} (for fully ionized gold) down to 10^{17} cm^{-3}. The 0.002–ps time step is $224\,\omega_p^{-1}$ at the high density, and $0.33\,\omega_p^{-1}$ at the critical density for CO_2, i.e., at 10^{19} cm^{-3}. So the problem will be strongly implicit in the solid, but might well be treated explicitly in the corona—our hybrid implicit algorithm successfully manages the transition. At the lowest background thermal temperature employed, $T_c = 1$ eV, and at 10^{24} cm^{-3} electron density, the cell size is $\Delta x/\lambda_D = 3.2 \times 10^5$. At this temperature and 10^{19} cm^{-3}, $\Delta x/\lambda_D = 96$. For the 150-keV suprathermals at critical density, $\Delta x/\lambda_D = 2.4$, while at 10^{17} cm^{-3}, $\Delta x/\lambda_D = 0.244$—allowing roughly four cells charge separation at the edge of an expansion.

With log λ set to 6 in the Braginskii [14] collision formula, $\nu_c \Delta t = 2.7 \times 10^6$ for $T_c = 1$ eV and 10^{24} cm^{-3} electron density; at critical, $\nu_c \Delta t = 27$. However, when T_c rises to 100 eV, the critical density $\nu_c \Delta t$ value is 2.7×10^{-2}. Still, the 100-eV

electrons are moving at only 4.1 μm/ps, and their mean free path is only 0.3 μm, so $\Delta x/\lambda_{mfp} = 7.9$. In contrast, the mean-free-path of the 150-keV suprathermals through the 10^{24}-cm^{-3} background gold electrons is 7 μm, or roughly $3\Delta x$.

A. Drag, Scatter and Field Effects

Figure 1 collects results from a number of test runs with the model. Suprathermals were introduced at the vertical fiducial into fixed ion density profiles as depicted in frame (c). For clarity of exposition the electrons were emitted as a left-travelling beam moving at 75 μm/ps. This corresponds to an energy of about 25 keV. The [redacted] 10^{24} cm^{-3} into a slab region about 50 μm wide where the peak density is 10^{25} cm^{-3}. In the frame (a) calculation the suprathermals experience only drag, which reduces their speeds as they pass through the dense region. The left boundary is a mirror. Frame (b) shows the effects of both drag and scatter on the high energy particle electrons. The magnitude of the mean drift speed to the left is reduced, as with the drag alone, and a significant fraction of the incident beam has its u component of velocity reversed by the scatter. Finally, frames (c) and (d) show the cumulative effect of drag, scatter and electric field accelerations. The emission point and fiducial have been shifted to the 160-μm position. Frame (c) shows the hot density n_h, and a cold density n_c noticeably below Zn_i in the plateau region. The phase plot of frame (d) shows that the incident beam is coupled to the returning stream of background thermals by a two-stream instability in the first 30 μm of plateau region plasma. More generally, when the incident hot stream is less beamlike and closer to a Maxwellian

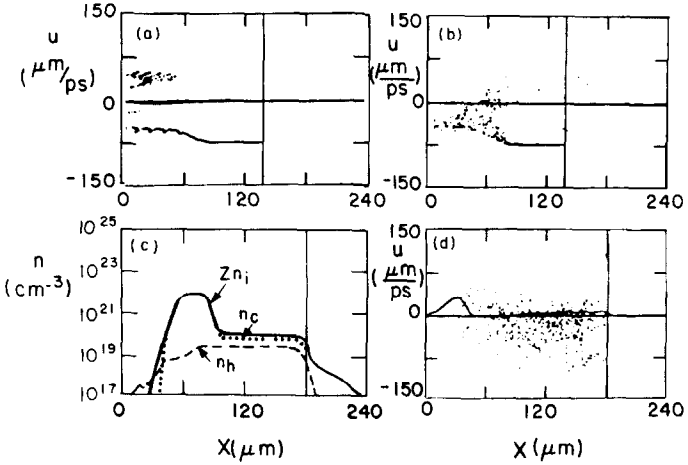

FIG. 1. Tests of suprathermal transport through a fixed ion background. (a) Beam penetration into an expanded slab. (b) Effects of drag and scatter. (c) The hot, cold and total electron densities under drag, scatter and with electric field effects after 2.5 ps. (d) Phase space plot of the hot electrons corresponding to frame (c); solid line is the cold drift speed.

with a temperature near the drift energy, two-stream effects are much less evident. Also, as the mean particle energy is raised appreciably beyond 25 keV, the localized effects of drag and scatter are much less discernable. Note that if details of the displayed two-stream effects were of particular interest, it would be advisable to rerun this example at reduced Δt, since with an excessive time step the moment method can distort the two-stream instability growth features [9, 11].

B. Thin and Thick Foils

Figure 2 shows the results for a foil illuminated by CO_2 light at a constant intensity of 3×10^{15} W/cm^2. We deposit 35% of this light and reflect the rest. The light enters from the right and deposits in the first cell with a density exceeding critical, i.e., where $Zn_i \geqslant 10^{19}$. The background temperature for thermal electrons and ions is initialized at $T_c = T_i = 1$ keV. The resonance absorption hot emission temperature for these conditions is about 35 keV; T_h has been fixed at this value.

The foil is 9.6 μm thick (four cells) and made of gold. We assume full ionization and set $Z = 79$; thus, the peak thermal electron number density Zn_i is 4×10^{24}. The

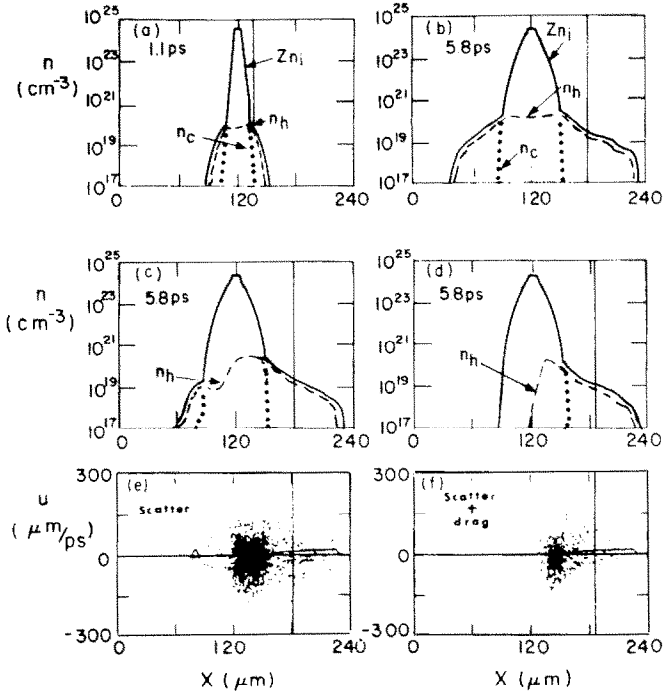

FIG. 2 A foil exposed to 35-keV emission. Frames (a) and (b) have the scatter and drag "off," but the field "on." In (c) the run has been made with scatter "on." For (d) the drag is included. The (e) and (f) phase plots correspond to (c) and (d), respectively.

thermal electron-ion coupling is very strong, such that $T_c = T_i$ in the center of the foil throughout the various runs. The proton–electron mass ratio has been artificially set to 10^2, instead of 1836, to economize and speed the evolution of the ion hydrodynamics.

Frames (a) and (b) are for scattering and drag "off," but the electric field "on." Here the vertical fiducial tracks the location of the critical surface. Frame (b) shows that by 5.8 ps the hot electrons have initiated fast ion blow-off on both sides of the foil. This early blow-off has moved nearly twice as far on the laser side. The fast ion density tracks the density of the hot electrons, which peaks at over 10^{20} cm^{-3}, or 10 times critical, in the center of the foil. Thermal electrons are strongly excluded from the fast ion regions. These electrons do drive a slow expansion of the main body of the foil, however, so that the $Zn_i = 10^{20}$ cm^{-3} points have moved some 20 μm from their initial positions.

In the run for frames (c) and (e) we have turned on the scatter as well as the electric field. The density of the 35-keV suprathermals then drops by more than a factor of 10 across the foil. From the phase plot (e), it is evident that the scatter is still holding most of the suprathermals on the laser side of the foil at $t = 5.8$ ps. Some have penetrated, however, to initiate a fast ion expansion, peaking at $Zn_i = 10^{19}$ cm^{-3} on the back side. Frames (d) and (f) show the results at the same time, 5.8 ps, when the effects of drag on the suprathermals are included. In this case the suprathermals are totally confined to the laser side of the foil. The phase plot shows a significant reduction in the number of particle hot electrons, since many have been slowed to low speed and absorbed in the background. Relatedly, the number with negative, foil-entrant u components significantly exceeds the number with $u \geqslant 0$.

It is important to note that in all three runs with 35-keV suprathermals, the critical surface at late time lies well out in the corona, where there are no thermal electrons. Thus, strictly speaking, there are no colds to be heated. This means that we have assumed a hot temperature that is unrealistically low. The model presently manages this situation by reducing the weights of the local suprathermals at critical to conserve charge, as it emits new suprathermals. However, since the emission temperature and energy are fixed, energy is not conserved. In a later version of the model, the emitted hots will be given a higher temperature to account for the energy born by the colder suprathermals they replace. For the present, however, we correct the deficiency in subsequent examples by going to markedly higher emission temperatures than those suggested by the resonance absorption formula [12]. This need for higher temperatures is consistent with recent CO_2 experiments.

C. 150-keV *Transport*

The emission temperature was raised to 150 keV for the Fig. 3 run, while the foil thickness was reduced to 4.8 μm (two cells), and its initial temperature was decreased to 1 eV. We continue to assume full ionization, $Z = 79$, for simplicity, although a more comprehensive treatment, in which Zn_i would start at low values and come up as T_c rose, is certainly desirable and planned for future studies. The lower T_c markedly increases the initial resistivity of the foil. However, frame (c) shows that the

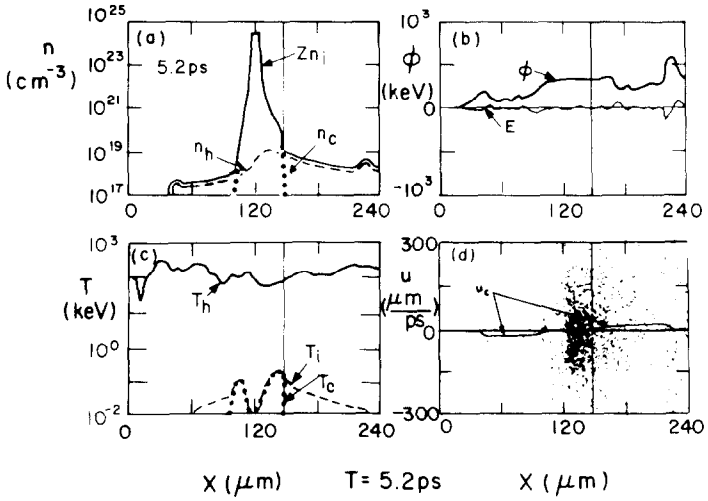

FIG. 3. 150-keV suprathermal transport through a 4.8-μm foil, initially with $T_c = T_i = 1$ eV. T_h is 150 keV, and the hot density is consistently below 10^{19} cm^{-3} outside the foil in frame (a). (b) The electrostatic potential in keV, and the electric field in arbitrary units. The potential approaches $3T_h$. (c) The hot and cold electron and ion temperatures. (d) The hot electron distribution in phase space.

drag deposition and Joule heating effects rapidly raise the coronal thermal and ion temperatures to the 100-eV range, reducing this resistivity.

Frame (a) verifies that with the higher T_h the critical surface shifts left to rest on the cold electrons, and the coronal hot density is substantially reduced to levels below about 10^{19} cm^{-3}. The calculation now consistently converts the colds to hot electrons. Frame (b) shows that a potential on the order of $3T_h$ develops to maintain the quasi-neutrality of the system. It also displays the active electric field in relative units. The phase plot (b), and also the n_h profile in (a), demonstrates that the electric field does act with some success to constrain the hot electrons to the laser side of this thinner foil. Frame (c) verifies that T_h ranges between 100 and 200 keV across the foil.

The inhibiting effect of resistivity in the cold central region of the foil is less than anticipated and will be explored more carefully with finer zoning, for example, in future work. Evident here, however, is the fact that the very energetic electrons present in the tail of a 150-keV suprathermal spectrum can penetrate very large resistive potentials, indeed, while eventually reflecting off the sheaths of a foil. Their return motions after these reflections can then cancel much of any net directed drift current through resistive barriers, leading subsequently to a lowering of such barriers.

D. Two-Foil Vacuum Insulation

As a final application of the model, we discuss the closure of a vacuum gap between two foils. In Fig. 4, to the foil previously discussed, we add a second identical foil separated by 60 μm. The laser illumination conditions are unchanged. Frame

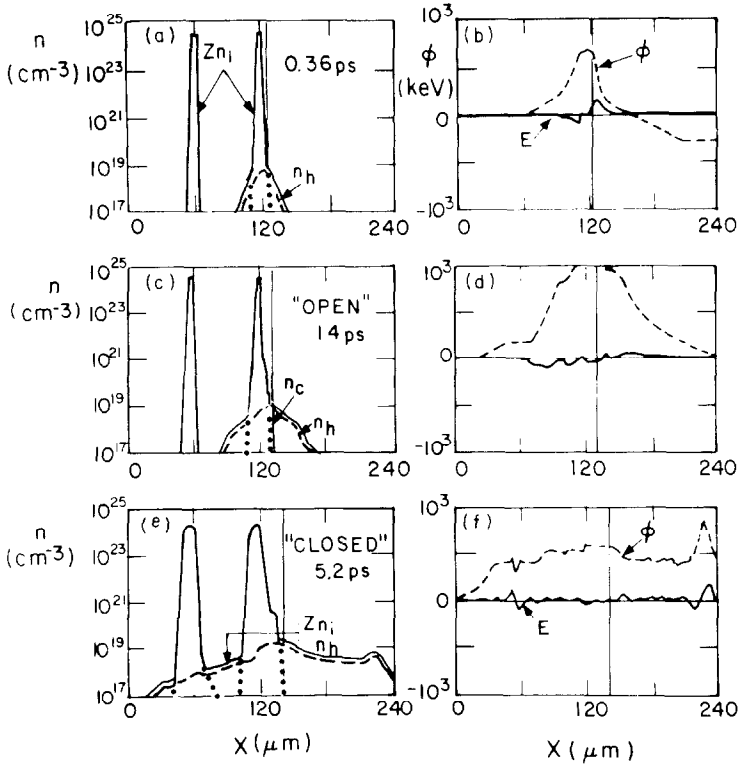

FIG. 4. The closure of a vacuum gap. The hot electrons move with the first-foil ions, then freely penetrate the second foil to continue in a fast ion expansion at its rear.

(c) shows that the gap between the foils is still open at 1.4 ps, while it is closed in frame (e) at 5.2 ps (this is about 25 ps at the physical m/M). In fact, there is then little difference between the n_h profile with or without (as in Fig. 3) the presence of the second foil. We had anticipated the possible development of a potential barrier to the hot electrons, as they first began to penetrate the second foil. This is not in evidence, again possibly due to the very long range for the 150-keV suprathermal tail.

4. CONCLUSIONS

A hybrid electron transport model has been outlined, in which collisional-PIC suprathermal electrons are moved self-consistently through background fluids of mutually colliding thermal electrons and ions. Implicit electric fields permitting economical calculations are obtained by the Implicit Moment Method. The particle description for the suprathermals assures the adequate modeling of effects dependent

on the detailed hot electron distribution. The directions to be followed for an eventual two-dimensional generalization of this description are also quite clear, particularly from the work of Brackbill and Forslund. The addition of fluid-ion and thermal-electron treatments allows for modeling over the full range of background densities required for global pellet simulations.

The utility of this approach has been demonstrated with applications to CO_2-generated transport in simple foil geometries. An immediate outgrowth of these applications is the result that the moderate suprathermal electron temperatures anticipated with resonant absorption are too low to allow for the self-consistent conversion of cold background thermal electrons into suprathermals. This difficulty is eliminated with 0 (150 keV) suprathermal emission, in agreement with recent CO_2 experiments. Simulations run with these hotter suprathermals show them to be extremely penetrating, and apparently capable of closing the gaps in vacuum insulation with no anomalies. This, however, is inconsistent with recent experimental data which now suggests some considerable inhibition of the suprathermals. Thus, more detailed application of the model, with, for example, much finer zoning and improved ionization physics, is in order, as is a two-dimensional generalization to explore the effect of magnetic fields in the presence of thermal electron resistive effects.

ACKNOWLEDGMENTS

The author is grateful to J. Brackbill, J. Saltzman, D. Forslund and C. Cranfill at Los Alamos and to J. C. Adam at École Polytechnique for many helpful and stimulating discussions during the course of this work. Thanks are also gratefully given to B. Cohen at Livermore for his careful reading of the original manuscript.

REFERENCES

1. R. L. MORSE, *in* "Methods of Computational Physics" (B. Alder, B. Fernbach, and M. Rotenberg, Eds.), Vol. 9, p. 213, Academic Press, New York, 1970.
2. R. J. MASON, *Phys. Fluids* **23** (1980), 2204; *Phys. Rev. Lett.* **43** (1979), 1795; and *in* "Laser Interactions And Related Plasma Phenomena," Vol. 5 (Proceedings, Fifth Laser Workshop on Laser Interactions with Matter, Rochester, NY, Nov. 5–9, 1979), Plenum, New York, 1981.
3. R. J. MASON, *in* "Proceedings of the ANS/ENS International Topical Meeting on Advances in Mathematical Methods for Nuclear Engineering Problems," Munich, West Germany, April 27–29, 1981.
4. R. SHANNY, J. M. DAWSON, AND J. M. GREENE, *Phys. Fluids* **10** (1967), 1281, and *Phys. Fluids* **12** (1969), 2227.
5. R. A. GENTRY, R. E. MARTIN, AND B. J. DALY, *J. Comput. Phys.* **1** (1966), 87.
6. D. L. BOOK, J. P. BORIS, AND K. HAIN, *J. Comput. Phys.* **18** (1975), 248.
7. S. T. ZALESAK, *J. Comput. Phys.* **31** (1979), 335.
8. R. J. MASON, *J. Comput. Phys.* **41** (1981), 233.
9. J. DENAVIT, *J. Comput. Phys.* **42** (1981), 337.
10. A. FRIEDMAN, A. B. LANGDON, AND B. I. COHEN, *Comments Plasma Phys. Cont.* **6** (1981), 225, AND A. B. LANGDON, B. I. COHEN, AND A. FRIEDMAN, *J. Comput. Phys.*, in press.

11. J. U. BRACKBILL AND D. W. FORSLUND, *J. Comput. Phys.* **46** (1981), 271.
12. D. W. FORSLUND, J. M. KINDEL, AND K. LEE, *Phys. Rev. Lett.* **39** (1977), 385.
13. R. JONES, private communication.
14. S. I. BRAGINSKII, *Rev. Plasma Phys.* **1** (1965), 205.
15. C. HIRT, *J. Comput. Phys.* **2** (1968), 339.
16. F. HARLOW, recommended in private communication.
17. L. G. SPITZER, "Physics of Fully Ionized Gases," Wiley, New York, 1961.
18. R. J. MASON, *Phys. Fluids* **14** (1971), 1943.
19. J. C. ADAM, A. GOURDIN SERVENIERE, AND A. B. LANGDON, *J. Comput. Phys.* **47** (1982), 229.